DOI: 10.1002/chem.200802008

Supramolecular Assembly of Self-Labeled Amphicalixarenes

Miriam S. Becherer,[a] Boris Schade,[b] Christoph Böttcher,*[b] and Andreas Hirsch*[a]

Abstract: The synthesis and precise supramolecular organization of new amphicalixarene **4** bearing four rodlike aligned fluorescent terephthalic benzamide moieties in the upper rim is reported. The aggregation of **4** was monitored by a combination of fluorescence, conductometry, and cryo-TEM measurements at different pH values and revealed significant structural differences. Most interestingly, we found that exactly 12 molecules of **4** assemble to form a spherical and structurally persistent micelle at pH 7, which coexists with rodlike micelles. In contrast to other examples of structurally defined micelles reported previously, this new type of self-labeled amphiphile serves as a fluorescence reporter with the terephthalic units additionally providing an extended cavity structure in the hydrophilic part, which facilitates the inclusion of guest molecules. In addition to the observed formation of well-defined micelles, the other highly important finding from this study is the fact that guest molecules directly influence the micellar organization because they can interact with both the free amphiphiles below the critical micelle concentration (cmc) or the micellar aggregate itself. These two types of interactions are especially pronounced in the case of the cationic pyrene derivative **10**, which binds electrostatically with the amphiphile **4**. In addition, a very unique membrane structure exhibiting a regular hexagonal pattern of 5 nm pores is formed by **4** at pH 4.

Keywords: amphiphiles · calixarenes · fluorescence spectroscopy · micelles · scanning probe microscopy

Introduction

Recently, we introduced the T-shaped dendrocalixarene **1**, which consists of two second-generation Newkome-type dendrons bearing 18 carboxylic termini at the upper rim and four dodecyl chains at the lower rim spatially aligned by the calixarene cage. This T-shaped calixarene is able to form structurally precisely defined micelles, which has allowed a detailed description of the three-dimensional architecture of a micelle with molecular precision for the first time.[1] The aggregate structure was determined from cryo-TEM images by employing image-processing and 3D reconstruction techniques and revealed an almost spherical aggregate of 7.5 nm diameter formed by seven molecules of **1** in a special C_2-symmetrical arrangement. The negatively charged carboxylic groups are homogeneously distributed over the surface of the micelle by nonlinear repulsive forces. Thus the T-shape of **1** induces pronounced backfolding and thereby reduced flexibility in the aggregate. The dodecyl chains of **1** are directed towards the core of the micelle, which can additionally accommodate hydrophobic guests. This behavior was proven by steady-state fluorescence experiments with pyrene, which showed that it is solubilized in the micelles of **1** sensing moderate polarity as concluded from the 11:13 ratio.[2] In subsequent investigations we discovered further examples of structurally defined and shape-persistent micelles composed of amphiphilic derivatives of C_{60} (**2** and **3**) bearing a [5:1] and [3:3] hexa-addition pattern, respectively. In both cases it was also possible to determine three-dimensional structural information from the detected assemblies, with two different ultrastructures being found for **2**, namely rodlike assemblies and spherical micelles, depending on the pH conditions.[3,4]

Herein, we present a new prototype of an amphiphilic calixarene **4**, which is self-labeled with four fluorescent terephthalic acid moieties covalently intercalated between the

[a] Dipl.-Chem. M. S. Becherer, Prof. Dr. A. Hirsch
Department of Chemistry and Pharmacy
Interdisciplinary Center of Molecular Materials (ICMM)
Friedrich-Alexander-Universität Erlangen-Nürnberg
Henkestrasse 42, 91054 Erlangen (Germany)
Fax: (+49) 9131-852-6864
E-mail: andreas.hirsch@chemie.uni-erlangen.de

[b] Dr. B. Schade, Priv.-Doz. Dr. C. Böttcher
Research Center for Electron Microscopy
Department of Chemistry and Biochemistry, Freie Universität Berlin
Fabeckstrasse 36a, 14195 Berlin (Germany)
Fax: (+49) 30-838-56589
E-mail: bottcher@chemie.fu-berlin.de

Supporting information for this article is available on the WWW under http://www.chemeurj.org/ or from the author.

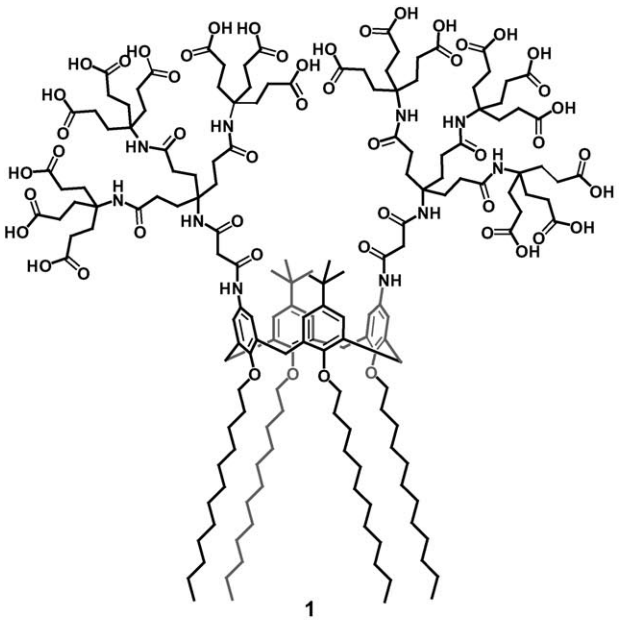

1

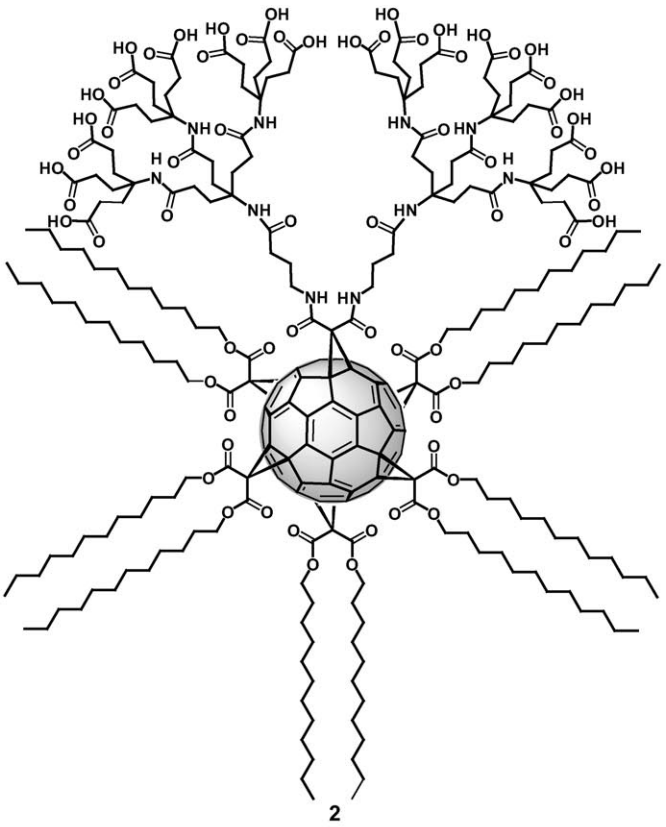

2

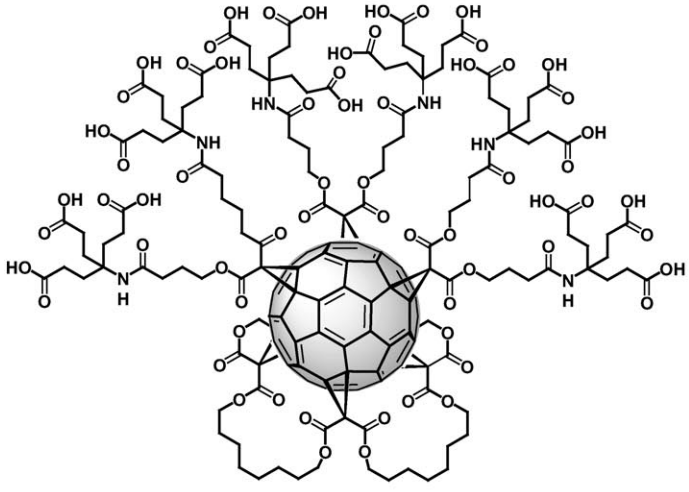

3

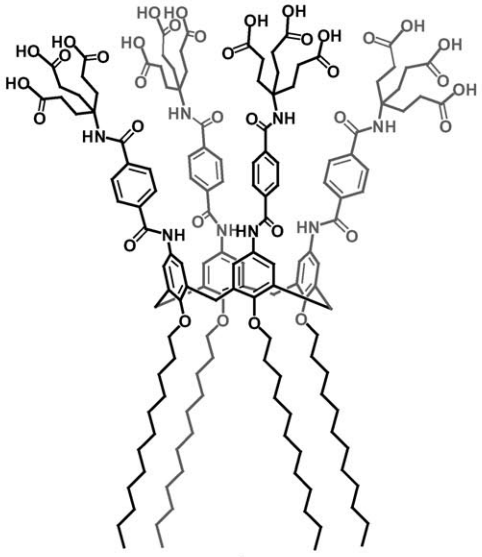

4

upper calixarene rim and the dendritic head groups. The basic idea was to introduce a couple of beneficial features that can be exploited to allow an even more detailed investigation of the micellization process. First, the chromophoric benzamide groups provide an internal fluorescence probe, which guarantees direct spectroscopic observation of micelle formation. Second, the comparatively enhanced rigidity combined with the high contrast properties provided by the aromatic building blocks attached to the head groups was expected to yield supramolecular assemblies with even more stability and thus better quality cryo-TEM data, which in principle are of comparatively low contrast. In addition, these units provide an extended cavity structure at the upper rim, which is expected to facilitate the inclusion of guest molecules.

The chromophoric benzamide absorbs at around $\lambda_{max} = 330$ nm.[5,6] In steady-state fluorescence measurements benzamide shows a pronounced Stokes' shift and emits in the region between 470 and 520 nm. As a consequence, the micellization of **4** is easily detectable without the addition of extra fluorescent reporters that could interfere with the exact mode of micellization. In addition to fluorescence spectroscopy we report on conductometry measurements as an independent measure of the aggregation behavior and the determination of the critical micelle concentration (cmc) of **4** in water. We also report on the complementary use of pyrene as a noncovalently bound fluorescence probe to determine the micropolarity of micelles of **4** in steady-state fluorescence measurements. The studies were carried out at pH 7 and 9 to investigate the putative effects on aggregation. We report also on the influence of charged pyrene derivatives **10** and **13** (see Scheme 2) on the formation of micelles to gain more information on guest–host interactions. Transmission electron microscopy (TEM), especially cryo-TEM, was used to gather direct structural information on the structure of supramolecular assemblies formed by **4** at pH values of interest and in the presence of guest molecules such as pyrene.

Results and Discussion

The synthesis of the new water-soluble dendrocalixarene **4** is shown in Scheme 1. The precursor calix[4]arene **5** was synthesized according to reported procedures.[7] To couple the fluorescent units to the upper rim, **5** was allowed to react with methyl 4-(chlorocarbonyl)benzoate (**6**) in THF. The ester groups of **7** were subsequently deprotected with lithium hydroxide in a water/THF mixture at elevated temperatures. The free carboxylic acids of **8** were attached to the Newkome dendrimers under standard Steglich conditions. The pure product **9** was produced by reprecipitation in a yield of 58%. The final step in the synthesis of this new fluorescent calixarene **4** was the cleavage of the *tert*-butyl esters with formic acid to introduce 12 free carboxylic acid groups.

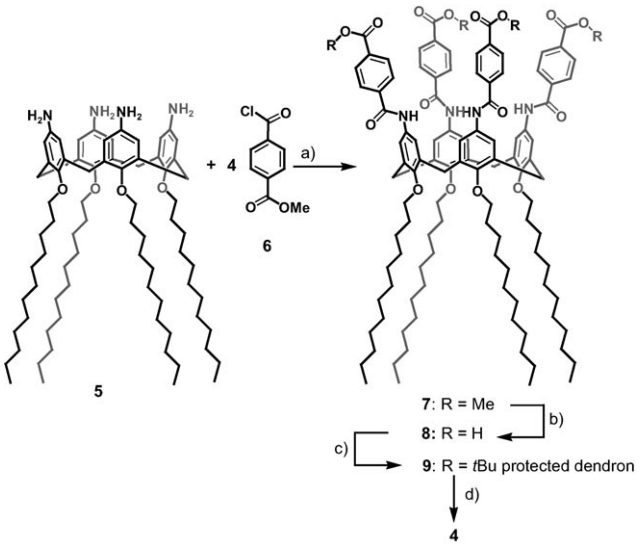

Scheme 1. Synthesis of the terephthal calixarene **4**. Reagents and conditions: a) i. $SOCl_2$, DMF, 70 °C, 4 h; ii. THF, −10 °C to room temperature; b) LiOH, H_2O, THF, 6 h, 60 °C; c) EDC, HOBt, DMAP, DMF, 0 °C to room temperature, 72 h; d) formic acid.

All new compounds were fully characterized by ^1H and ^{13}C NMR spectroscopy, elemental analysis, and mass spectrometry. The free acid **4** is soluble in phosphate-buffered water at pH 7 or higher, but not in apolar solvents.

The functionalized pyrene **10**, which was used in the fluorescence measurements as a fluorescence antenna, was synthesized according to Scheme 2. The hydroxy group of commercially available 4-(pyren-1-yl)butanol (**11**) was replaced by bromide in a nucleophilic substitution reaction.[8] Subsequently, the bromide of **12** was substituted by trimethylamine in THF. The resulting ammonium salt **10** was purified by reprecipitation. This positively charged pyrene derivative **10**, pyrene, and 4-(pyren-1-yl)butyric acid (**13**) were used to investigate the aggregation ability of the terephthal calixarene **4**.

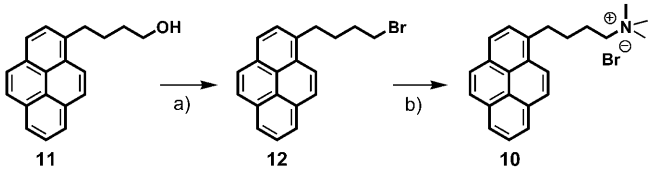

Scheme 2. Synthesis of 1-(4-trimethylammoniobutyl)pyrene bromide (**10**): Reagents and conditions: a) CBr_4, PPh_3, CH_2Cl_2, 6 min; b) NMe_3, THF, 8 h.

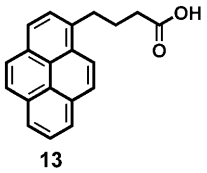

Characterization of the aggregation of 4: Excited at $\lambda = 333$ nm, deprotonated $\mathbf{4}^{12-}$, generated by the action of 12 equivalents of NaOH, emits radiation of around 490 nm. The light emission is caused by twisted intramolecular charge transfer (TICT).[9] This TICT arises either from electron transfer between twisted donor–acceptor groups or from a change in the configuration of the amino nitrogen from pyramidal to planar in the ICT. Fluorescence spectra of $\mathbf{4}^{12-}$ are shown for a concentration range between 4.5×10^{-8} and 2.7×10^{-4} mol L^{-1} in Figure 1. The absorption spectrum of $\mathbf{4}^{12-}$ is displayed in the inset.

The fluorescence spectra show an increase in intensity of the benzamide band (I_{BA}) on increasing the concentration of **4** until a maximal intensity (f) is reached. I_{BA} strongly decreases on further increasing the concentration of **4**. A plot of this nonlinear behavior of I_{BA} as a function of the concentration of **4** shows a fluorescence intensity maximum at 2.2×10^{-5} mol L^{-1} of **4** (Figure 2).[10]

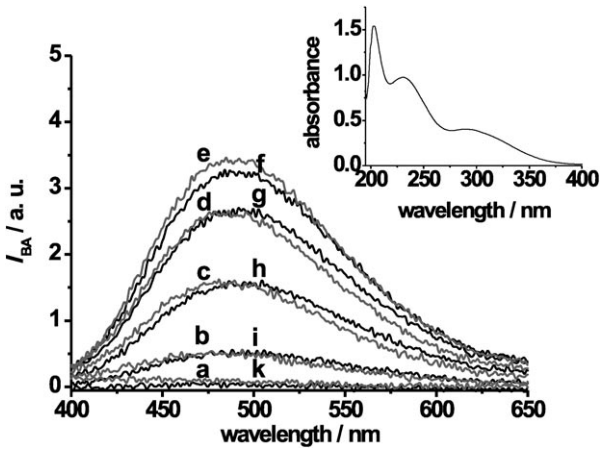

Figure 1. Intensity of the benzamide band I_{BA} of $\mathbf{4}^{12-}$ in water at low (a) 4.5×10^{-8}, b) 9.1×10^{-7}, c) 3.9×10^{-6}, d) 8.2×10^{-6}, e) 1.7×10^{-5}, f) 3.5×10^{-5} mol L^{-1} (gray lines)) and high (g) 5.1×10^{-5}, h) 8.7×10^{-5}, i) 1.5×10^{-4}, k) 2.7×10^{-4} mol L^{-1} (black lines)) concentrations of **4** ($\lambda_{ex}=333$ nm; inset: absorption spectrum of **4**).

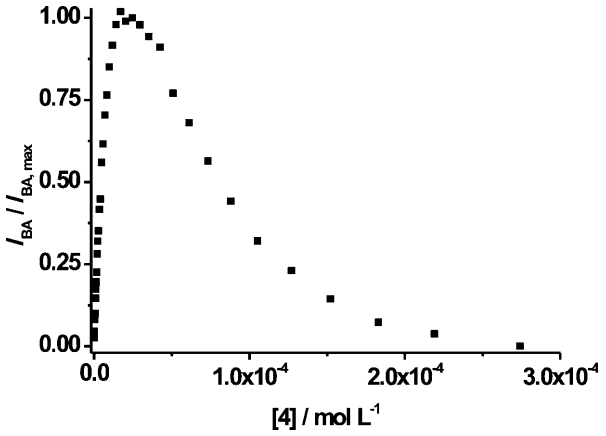

Figure 2. Intensity of the benzamide band I_{BA} of $\mathbf{4}^{12-}$ at 485 nm versus the concentration of $\mathbf{4}^{12-}$ in pure water ($\kappa=2$ μS, $\lambda_{ex}=333$ nm).

The initial increase in I_{BA} is due to the steady increase in the calixarene concentration. Beyond the maximum the fluorescence energy is quenched by energy transfer between the benzamide moieties, which come into close proximity on micelle formation. Hence, we associate the maximum of the fluorescence with the cmc of amphicalixarene **4** (cmc_0), that is, 2.2×10^{-5} mol L^{-1}.

To support this result the cmc_0 was also determined by conductivity measurements. The reliability of this method was initially proven by determination of the known cmc of sodium dodecyl sulfate (9.0×10^{-3} mol L^{-1}), which is in good accord with the literature value within the limits of experimental error (8.1×10^{-3} mol L^{-1}).[11] The conductivity of the calixarene $\mathbf{4}^{12-}$ solution increased linearly with concentration in two sections, and can be fitted by two straight lines (Figure 3). Their intersection at a concentration of 2.3×10^{-5} mol L^{-1} coincides within experimental error with the value of cmc_0 determined by fluorescence spectroscopy.

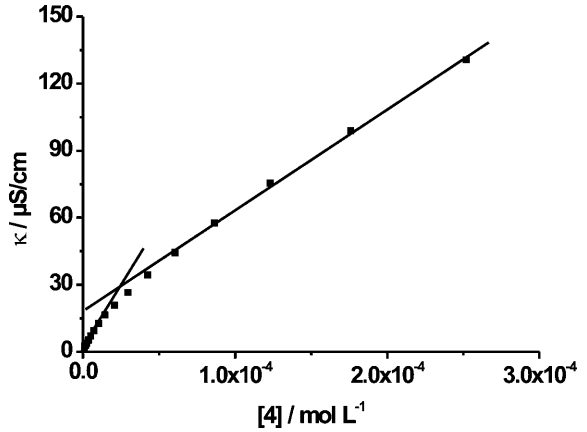

Figure 3. Variation of conductivity versus the concentration of $\mathbf{4}^{12-}$ for the determination of the cmc in pure water ($\kappa=2$ μS, $T_{ref}=25$ °C).

Accordingly, the amphicalixarene **4** was investigated without auxiliary dyes in buffered water at pH 7 (Na/K phosphate) and 9 (Na borate), respectively. The benzamide emission band experiences a shift to 485 nm at pH 7 and to 496 nm at pH 9, respectively, which demonstrates its sensitivity towards the solvent environment.[9] The plots of $I_{BA}/I_{BA,max}$ as a function of the concentration of **4** (Figure 4) follow qualitatively the same trends as those determined for **4** treated with 12 equivalents of NaOH.

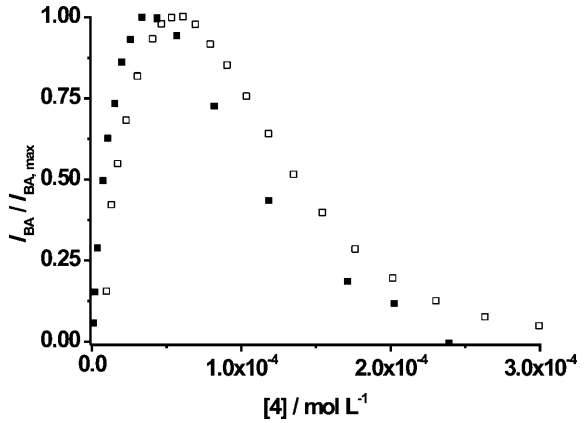

Figure 4. $I_{BA}/I_{BA,max}$ of **4** versus the concentration of **4** at pH 7 (□) and 9 (■).

Low fluorescence intensities for the benzamide moieties are observed at both pH values at high concentrations of **4**, which indicates a close spatial association of the benzamide units within the aggregates. At pH 7, the cmc of **4** (cmc(**4**)) is 5.0×10^{-5} mol L^{-1} and a value of 3.7×10^{-5} mol L^{-1} determined at pH 9. The smaller cmc(**4**) value at pH 9 compared with neutral conditions indicates a modified interaction between the chromophores and hence a different structural organization. Electron microscopy studies indeed showed different aggregation behavior depending on the pH (see below). Both cmc values are higher than in pure water

(Table 1). Hence, the different buffer salts and the resulting change in ionic strength, as well as different pH values, modify the aggregation behavior of calixarene **4**.

Table 1. Critical micelle concentrations (cmcs) of **4** at pH 7 and 9 and the intersection points of the linear analysis of the I_1 intensities of pyrene, **10**, and **13**.

	cmc of **4** [mol L^{-1}]		Intersection points [mol L^{-1}] of the linear fitted slopes of I_1/I_0 for the pyrene moiety of pyrene, **10**, and **13** versus [**4**][a]	
cmc_0	2.3×10^{-5}			
	pH 7.0	pH 9.0	pH 7.0	pH 9.0
cmc(**4**)	5.6×10^{-5}	3.7×10^{-5}		
cmc($\mathbf{4_{py}}$)	4.1×10^{-5}	2.1×10^{-6}	8.0×10^{-6}	6.0×10^{-6}
cmc($\mathbf{4_{10}}$)	7.3×10^{-5}	5.2×10^{-5}	4.2×10^{-7}	3.0×10^{-7}
cmc($\mathbf{4_{13}}$)	4.0×10^{-5}	4.3×10^{-5}	1.9×10^{-5}	2.4×10^{-5}
cmc(**10**)	6.3×10^{-5}	–	–	–
cmc(**13**)	1.0×10^{-4}	–	–	–

[a] See ref. [12].

Structural characterization by electron microscopy: As has been extensively shown in previous publications[1,3,4] cryo-TEM provides direct and detailed evidence of the aggregate formation of amphiphilic dendrimers. However, the low contrast associated with this technique is a big problem and requires the additional application of image-averaging techniques or the use of contrasting materials. In this work, the introduction of benzamide entities boosts the contrast and allows a better visualization of the aggregates without further treatment of the data (Figure 5).

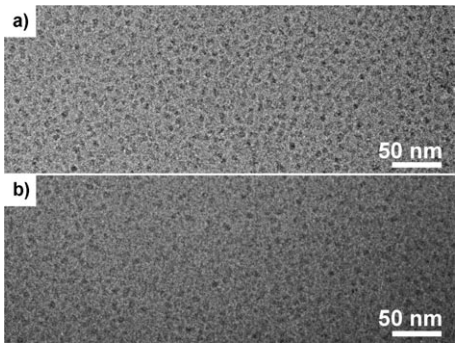

Figure 5. The introduction of aromatic terephthalamides into **4** causes visibly enhanced contrast in the cryo-TEM images of micellar assemblies (a) compared with those of dendrocalixarene **1** without the aromatic spacer (b).

All samples used for TEM had a concentration between 7.5×10^{-4} and 10.4×10^{-4} mol L^{-1}, which is clearly above the value of cmc(**4**). The aggregates visualized by cryo-TEM showed different structures depending on the pH. At pH 7 (Na/K phosphate-buffered), rodlike and spherical micelles were observed to coexist (Figure 6a). Both types of aggregates exhibit low density areas in their central part, which can be attributed to the hydrophobic core, a typical structural feature of double-layered amphiphilic architectures. The rodlike micelles have a diameter of around 7.1 nm, which is only slightly larger than twice the length of the fully stretched molecule (3.2 nm), which also hints at the double-layer arrangement of the amphiphiles. In contrast, the spherical micelles are slightly larger with a diameter of around 8.4 nm (a volume that allows 12 molecules of **4** to be accommodated, as discussed below). We conclude that the molecular packing is slightly different in both of these aggregates, which allows two types of curvature. This observation is very similar to our earlier examinations of dendrofullerene **2**,[3] which forms rodlike and spherical micelles depending on the pH of the solutions.

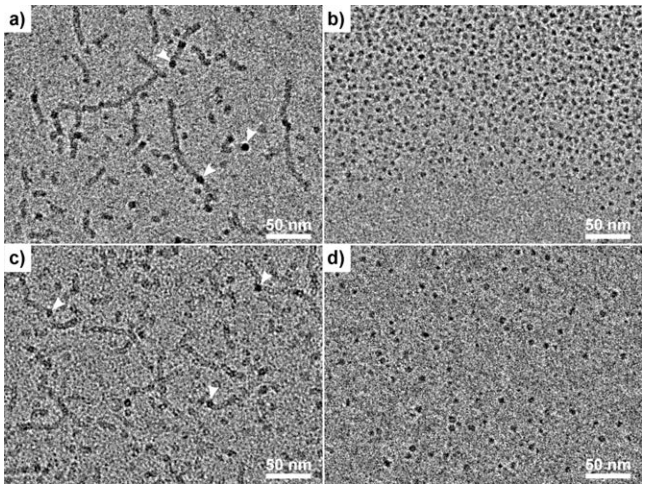

Figure 6. Typical cryo-TEM images of **4** in buffered water at different pH values and in the presence of pyrene. Pure **4** forms predominantly rodlike and spherical micellar aggregates at pH 7 (a) and only almost uniform spherical micelles at pH 9 (b). After the addition of pyrene the dimensions of the aggregates at pH 7 remain unaffected (c), whereas at basic pH the loaded micelles are less uniform providing a larger particle size distribution (d). The formation of micellar end-caps can be detected (see arrows in a and c) irrespective of the addition of pyrene.

Calixarene **4** forms solely spherical micelles at pH 9 (Na borate buffer), which, with an average diameter of only 6.3 nm, are clearly smaller than those at neutral pH (Figure 5b). From this data, it can be concluded that denser packing of the micelles occurs under basic conditions in comparison with the aggregates obtained at neutral pH. The resulting larger curvature may arise from greater bending of the dendrons as a result of mutual repulsion of the fully charged carboxylic groups at this pH value.

In comparison with our earlier investigations,[1,3,4] calixarene **4** exhibits slightly different aggregation behavior as we have evidently detected conditions (neutral pH) under which two different aggregation states are in equilibrium (compounds **1** and **2** show uniform entities exclusively at each pH). This observation coincides with the behavior found for classical detergents in which spheres and rods are occasionally found in equilibrium depending on the concentration,[13a] pH, and ionic strength.[13b] A typical structural feature, which indicates the different spatial demand of the

molecules in spheres and rods, are the swollen end-caps. They can also be found in the rods of **4** (see arrows in Figure 6a). The slightly increased diameter of the caps coincides well with the diameter of the spheres.

In addition, all the spherical aggregates of **4** display an ultrastructural organization similar to those of the structurally persistent micelles obtained from calixarene **1** or the dendrofullerenes **2** and **3**. A gallery of class averages proving this finding is provided in Figure 7a for the spherical micelles formed at pH 7. Each of the so-called class sum images in the gallery represents a different spatial orientation of the micelle. Taking these images together a complete three-dimensional structure determination of the aggregate can be achieved, as described previously.[1] Figure 7b shows the surface representation of the reconstruction based on a data set of 11041 images of individual aggregates.[14]

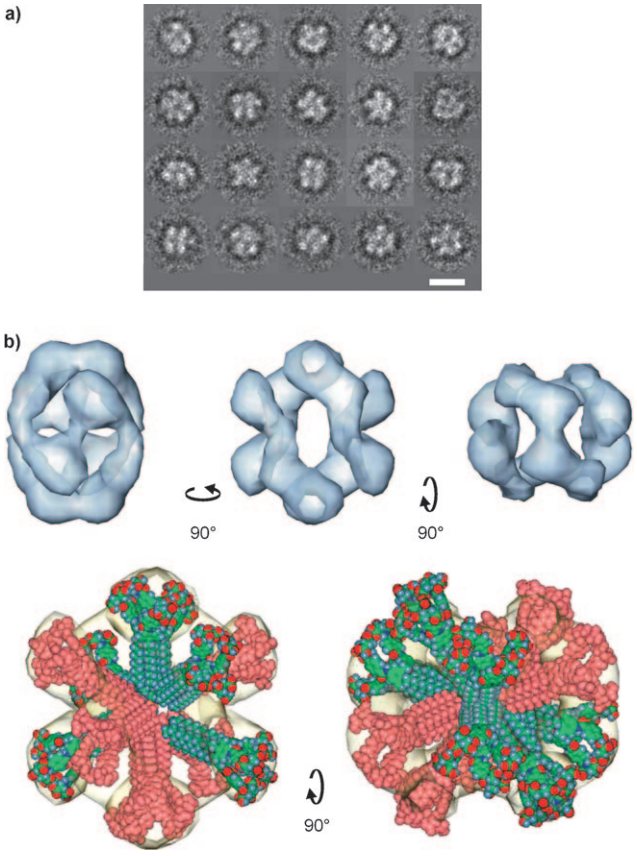

Figure 7. a) Selected reference free class sum images of 11041 individual aggregates gathered from electron micrographs of a cryo-negative stain (phosphotungstic acid stain) sample of **4** in buffered water at pH 7. The class sum images represent different spatial orientations of the three-dimensional micelles and show different density patterns and dimensions due to its inherent structure. b) Upper row: Transparent surface representation of the 3D density map calculated from 11041 images of individual micelles formed by **4** at pH 7.2. The reconstruction is shown in the direction of the inherent two-fold symmetry (D_2) axes. Lower row: Fitting of the molecular models of **4** to the 3D density map shown above. Twelve individual molecules of **4** can be very accurately accommodated in the reconstructed volume.

The 3D density map obtained shows the accommodation of 12 molecules in a perfectly D_2-symmetrical manner. This structure differs from that obtained from the structurally similar compound **1.** The packing of the head groups of **4** is denser in the aggregates, most probably due to the smaller head-group volume (first-generation dendrons in **4** versus second-generation dendrons in **1**). Figure 8 illustrates these differences.

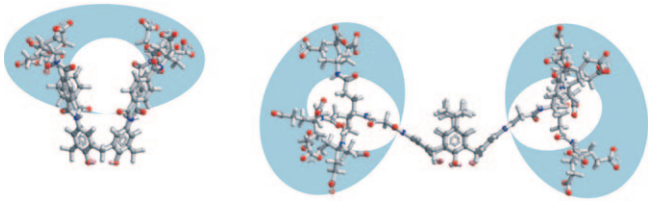

Figure 8. Spatial conformations of the head groups of **4** (left) and **1** (right) found in structurally persistent spherical micelles. The smaller space required by **4** allows denser packing of the second-generation dendritic head groups compared with the third-generation head groups in compound **1**.

Whereas the second-generation dendrons of **1** protrude widely in different directions (Figure 8, right), the less voluminous first-generation dendrons of **4** are packed more tightly (Figure 8, left), which allows a larger aggregation number of 12 compared with seven in the case of **1**.

A unique supramolecular architecture at pH 4: The results of the TEM analysis of **4** at pH 4 were both very interesting and surprising. As protonation of the head groups drastically reduces its solubility, slow precipitation is observed upon acidification. Although no ordered structural features were expected from the precipitate we studied the cloudy suspension by cryo-TEM. To our surprise very large and wrinkled membrane sheets of micrometer size appeared, which showed a regular pattern of pores with a uniform diameter of 5.0 nm. In those areas where the sheets were unwrinkled the hexagonal-ordered pattern of the pores became apparent (Figure 9).

The tilt series (−22.5 to 22.5° in 5° steps) of these cobweb-like aggregates reveal a membrane thickness of 6.0 nm if the sheets are orientated in a side-view orientation, for example, with its edges parallel to the electron beam (Figure 10, right).

One can therefore conclude that the network itself consists of interconnected cylindrical components, with a cross-section diameter of 6.0 nm, that undergo regular bifurcations. The cylinder diameter of 6.0 nm coincides well with the molecular double-layer dimension.

Similar porous membranes have recently been described by Kim et al.[15] for dumb-bell-shaped amphiphiles forming a regular hexagonal pattern of 25 nm pores, which can be thermoreversibly switched to form closed vesicles featuring a continuous membrane layer.

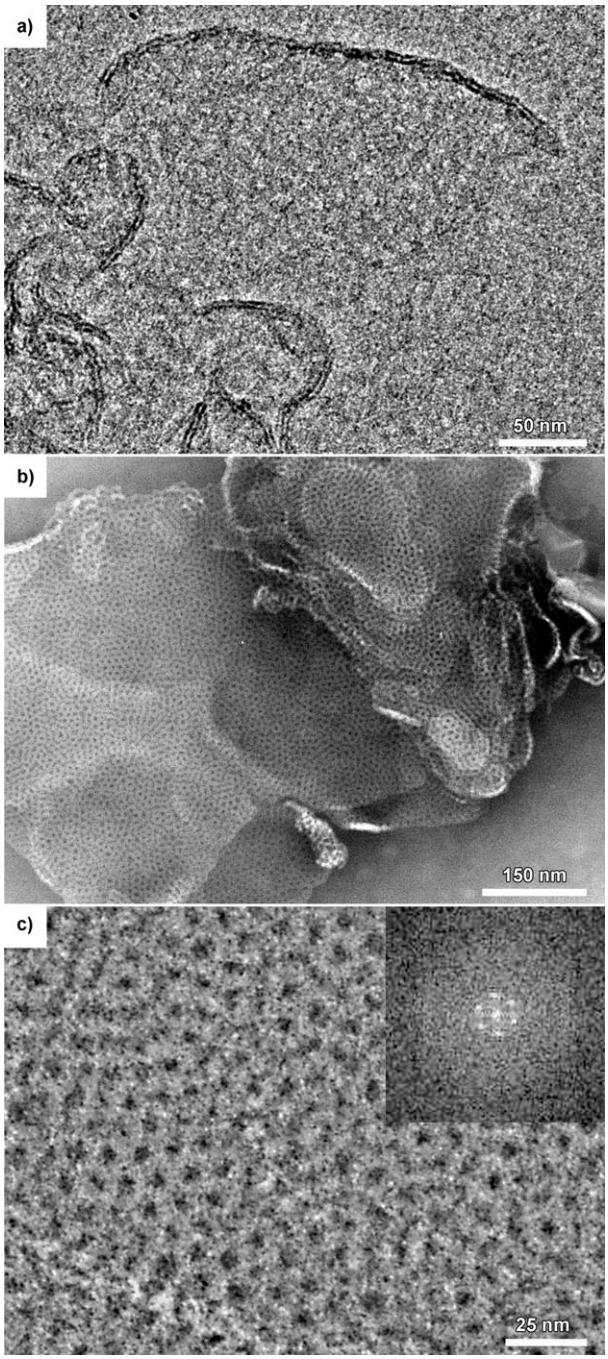

Figure 9. a) Cryo-TEM image and b) negatively stained (phosphotungstic acid) preparation of **4** at pH 4. A porous membrane is formed that shows pores of 5.0 nm diameter in a hexagonal arrangement, as shown by the magnified image and its corresponding Fourier transform in (c).

With these two remarkable examples of a new supramolecular architecture formed by very different molecules, the direction of future investigations is clear; the aim will be to show to what extent the ultrastructural organization of porous membranes is dependent on the molecular structure employed. It would be, for example, very interesting to investigate the potential of generating membranes with a tailor-made pore size.

Transport capacities of the amphicalixarene 4 aggregates: To examine the transport capacities and the possible effects of additives on the aggregation process, pyrene and its substituted derivatives **10** and **13** were used as guest molecules and probes in the presence of terephthal calixarene **4**. By utilizing these antennae, fluorescence experiments were performed at pH 7 and 9 at a constant concentration of 6.0×10^{-7} mol L^{-1} of the antennae.

Transport of pyrene: Upon excitation at 333 nm, in addition to the broad emission band of **4**, characteristic and well-defined vibronic emission bands of the pyrene moiety appear in the spectra (Figure 11). At pH 7 and 9 the benzamide bands are located at 485 nm and 495 nm, respectively.

I_{BA} increases on increasing the concentration of **4** and reaches a maximum at 4.1×10^{-5} mol L^{-1} (pH 7), which is attributed to the cmc of **4** in the presence of pyrene (cmc($\mathbf{4_{py}}$)) (Figure 12).[10] This value is slightly smaller than cmc(**4**). Beyond this point I_{BA} decreases again due to enforced intra- and intermolecular interactions within the micelles and eventually tends to zero. At pH 9 the benzamide bands of **4** show a slightly different behavior. I_{BA} rises up to a concentration of 2.1×10^{-6} mol L^{-1}, features a local minimum at 1.5×10^{-5} mol L^{-1}, and reaches a second maximum at 4.1×10^{-5} mol L^{-1}. This means that **4** starts to form aggregates at a concentration of 2.1×10^{-6} mol L^{-1}. At higher concentrations the fluorescence intensity is increasingly quenched due to the close contact of the benzamide moieties. At the next maximum (4.1×10^{-5} mol L^{-1}), a second cmc is obtained, which corresponds to the value of cmc(**4**) obtained at pH 7.

As the monomer emission of pyrene is highly sensitive to the polarity of the environment the intensity ratio between the first and third vibronic bands I_1 and I_3 can be used to monitor the polarity of the surrounding medium. In water this ratio is about 1.9 and in apolar solvents, like dodecane or hexane, it lies in the range 0.5–0.6.[16] In Figure 13 the fluorescence intensity ratios of pyrene (I_1/I_3) at pH 7 and 9 are plotted as a function of the concentration of **4**.

At low concentrations of **4** pyrene is predominantly located in the aqueous phase both at pH 7 and 9, as determined by the high I_1/I_3 ratio (1.9). At pH 7 the value of the I_1/I_3 ratio starts to decrease at around 8.0×10^{-6} mol L^{-1} of **4** and reaches a nearly constant value of 0.9 at 4.1×10^{-5} M, which is the value of cmc($\mathbf{4_{py}}$). At pH 9 the cmc of the micelles is indicated by a slight decrease in the I_1/I_3 ratio from 1.9 to 1.8. At both pH values the I_1/I_3 ratios suggest that the pyrene environment is more polar than a purely aliphatic environment ($I_1/I_3=0.5$–0.6). Thus, it can be concluded that pyrene is predominantly exposed to the more polar regions at the upper rim of the amphicalixarenes in their micellar aggregates and a pyrene alkyl chain interaction can be neglected. This observation is in accord with previous inclusion experiments with calixarene **1** and pyrene.[2]

An exponential decrease in the intensity is observed in the plots of the fluorescence intensities of the first vibronic band of pyrene (I_1) at pH 7 and 9 as a function of the concentration of **4** (see the Supporting Information). At the

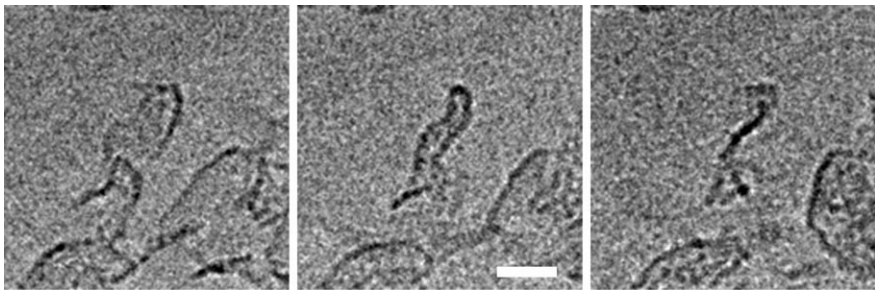

Figure 10. Cryo-TEM images showing in detail the porous membrane formed by **4** at pH 4 (cf. Figure 9) at different tilt angles (−22,5, 0, and +22,5° from left to right) revealing the membrane layer thickness of 6 nm (right) (bar: 50 nm).

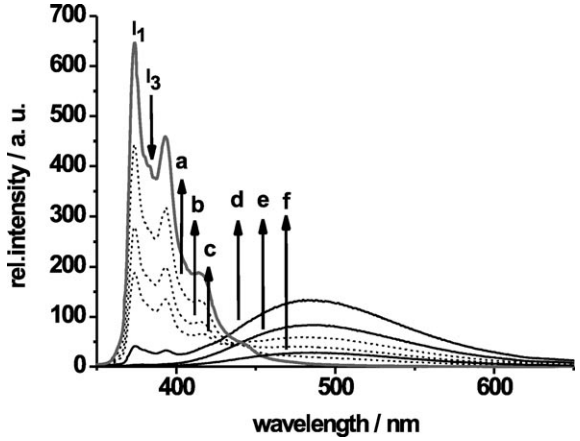

Figure 11. Fluorescence spectra of **4** in the presence of pyrene (6.10×10^{-7} mol L^{-1}) at varying concentrations of **4** (a) 1.9×10^{-6}, b) 4.8×10^{-6}, c) 7.2×10^{-6} (dashed lines), d) 8.2×10^{-6}, e) 3.1×10^{-5}, f) 5.3×10^{-5} mol L^{-1} (black lines)) and of 6.0×10^{-7} mol L^{-1} pyrene (gray line) in buffered solution at pH 7 ($\lambda_{ex}=333$ nm).

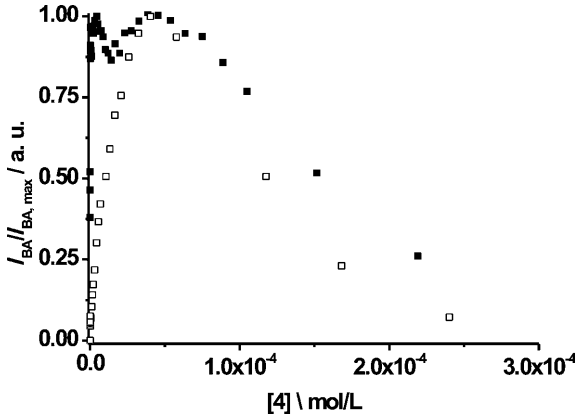

Figure 12. Intensity of the benzamide band I_{BA} of **4** versus the concentration of **4** in the presence of pyrene (6.10×10^{-7} mol L^{-1}) at pH 7 (□) and 9 (■).

lowest concentration of **4** (2.8×10^{-8} mol L^{-1}) I_1 is nearly equal to the I_1 intensity of pyrene in the absence of **4** at pH 7 and 9. The same quenching behavior was found for 1:1 complexes of poly(propyleneimine) dendrimers with pyrene.[18] Both the low and high concentration sections of these plots can be fitted by straight lines.[17] The intersection points of these lines are given in Table 1.

No excimer emission due to the formation of pyrene dimers is observed, which would be expected at around $\lambda_{max}=480$ nm.[5] Hence, under these conditions no aggregation of pyrene takes places within the micelles of **4** at either pH 7 or 9.

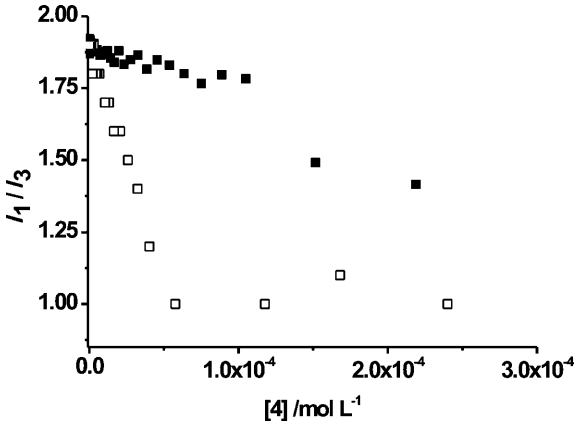

Figure 13. I_1/I_3 of pyrene versus the concentration of **4** at pH 7 (□) and 9 (■) in the presence of pyrene (6.10×10^{-7} mol L^{-1}).

It is possible that the structural effects of the aggregation of **4** at different pH values and a probable influence of guest molecules on the supramolecular organization of the host nanocontainers may be deduced from these detailed data. Cryo-TEM investigations should indicate if the addition of pyrene results in changes in the supramolecular organization of the micelles. Again the micrographs of the mixtures show rods and spherical micelles at pH 7 and only spherical micelles at pH 9 (Figure 6c). The average diameters of 8.2 nm for spherical micelles and 6.8 nm for rod-shaped aggregates coincide with those aggregate dimensions found for the unloaded micelles at pH 7, which suggests that these aggregates are not distorted upon the uptake of guest molecules. Swollen end-caps can also be detected, as in the unloaded micelles (see the arrows in Figure 6c).

Different behaviour was observed under basic conditions (Figure 6d). The loaded micelles are less uniform compared with the unloaded aggregates at the same pH. Although the average diameter of 6.8 nm is only slightly larger than the 6.3 nm for the unloaded micelles, a notable number of aggregates have diameters of the same magnitude as the spherical micelles at neutral pH (8.2 nm). As pointed out above, pyrene must be involved in a pyrene–dendron associ-

ation at the upper rim of **4**. Hence, interactions of the guest molecule with the dendrons might prevent them from bending as much as the unloaded micelles at basic pH. At this point it cannot be determined whether only the larger micelles are loaded with pyrene molecules or if different aggregates form as a result of the additive. Note that differences in diameters are also evident if the three-dimensional ultrastructure of structural-persistent micelles is contemplated. Depending on the spatial orientation of the object, the pattern of the projection image (TEM delivers projection images) is different and therefore small and large diameters can be seen.

These observations clearly show that pyrene, which is frequently used as a fluorescence label to determine the cmcs of amphiphiles, is not an innocent spectator, but plays an active role in the micellization process.

Transport of pyrene derivatives: To investigate this issue further we also studied the behavior of the pyrene derivatives **10** and **13** as guest molecules. At pH 7 and 9 these molecules carry one positive or one negative charge, respectively. Because these pyrene derivatives are themselves amphiphilic we first had to determine their cmcs and make sure that they were employed at concentrations below their cmcs in the subsequent host–guest investigations with **4**.[19] The cmc of **10** at pH 7 is 6.3×10^{-5} mol L^{-1} and that of **13** is 1.0×10^{-4} mol L^{-1}. Thus we prepared stock solutions of **10** and **13** with a concentration of 6.0×10^{-6} mol L^{-1} to ensure that they do not form micelles on their own. Fluorescence emission spectra ($\lambda_{ex}=333$ nm) show the expected vibronic structure characteristic of the pyrene chromophore between 374 and 445 nm as well as the expected benzamide emission of amphicalixarene **4** at around 490 nm. The cmcs of **4** in the presence of **10** and **13** (cmc($\mathbf{4_{10}}$) and cmc($\mathbf{4_{13}}$)) were obtained from plots of $I_{BA}/I_{BA,max}$ as a function of the concentration of **4** (Figure 14). The maximum values of the plots represent the corresponding cmcs (Table 1).

In all cases the cmcs are slightly different to those obtained for **4** in the absence of the guest molecules (cmc(**4**), cmc$_0$). In the presence of pyrene and negatively charged **13** the cmcs tend to be higher than cmc$_0$ with the exception of cmc($\mathbf{4_{py}}$) at pH 9. Significantly, cmc($\mathbf{4_{10}}$) is markedly higher than cmc(**4**). The positive charge on **10** seems to disfavor micelle formation, probably due to the formation of coulombic complexes between **4** and **10** at low concentrations of **4**. This electrostatic association has to be overcome or at least considerably disturbed during micelle formation in the presence of **10**. Of course, such electrostatically bound complexes are not expected to form with pyrene and **13**. The pronounced attractive interaction between the oppositely charged molecules **4** and **10** becomes especially apparent if one looks at the decay of the pyrene emission I_1 as a function of the concentration of **4** (Figure 15). Its decay, which is due to electronic communication between the two chromophores located in close proximity, proceeds almost instantaneously compared with the decay of **13**, even well below the cmc($\mathbf{4_{10}}$). This provides very strong corroboration for the suggestion that electrostatic coulombic complexes are formed between **4** and **10** prior to the micelle formation of **4**. Nevertheless no pyrene excimers were observed during the fluorescence experiments. This shows that the pyrene moieties are separated from each other. Hence, they are most probably located within the calixarene cavity. A linear curve analysis of the I_1 progression at high and low concentrations of calixarene **4** in the presence of **10** and **13** reveals intersection points for each pair of linear plots. The intersection points for **10** are at 4.2×10^{-7} mol L^{-1} at pH 7 and 3.0×10^{-7} mol L^{-1} at pH 9 (Table 1).

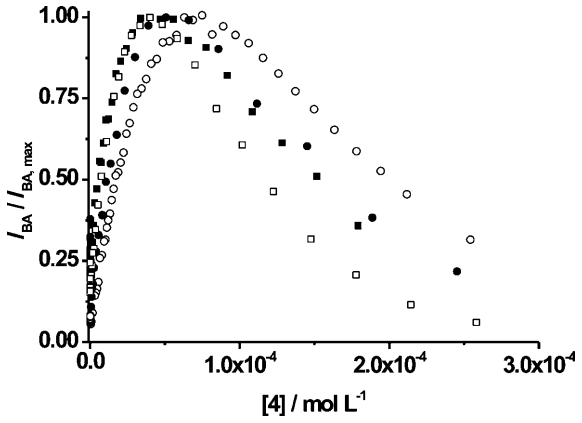

Figure 14. Intensities of the benzamide band I_{BA} of **4** versus the concentration of **4** in the presence of **10** (6.10×10^{-6} mol L^{-1}) at pH 7 (○) and 9 (●) and in the presence of **13** (6.10×10^{-7} mol L^{-1}) at pH 7 (□) and 9 (■).

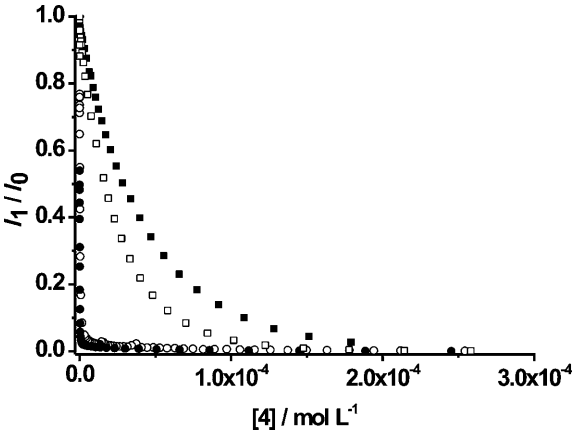

Figure 15. Intensity ratio I_1/I_0 of the pyrene-based emissions of **10** and **13** as a function of the concentration of **4** in the presence of **10** (6.10×10^{-7} mol L^{-1}) at pH 7 (○) and 9 (●) and in the presence of **13** (6.10×10^{-7} mol L^{-1}) at pH 7 (□) and 9 (■).

Conclusion

The structurally well-defined micelles of the new amphicalixarene **4** are the first to be studied in detail by a combination of fluorescence, conductometry, and cryo-TEM meas-

urements. In contrast to other examples of structurally defined micelles,[1,3,4] this general approach was facilitated by the presence of terephthalic acid moieties in the calixarene, which serve as fluorescence reporter units in this self-labeled amphiphile. One of the more important findings from this study is the fact that guest molecules directly influence the micellar organization because they can interact with both the free amphiphiles below the critical micelle concentration (cmc) or with the micellar aggregate itself. These two types of interactions are especially pronounced in the case of the cationic pyrene derivative **10**, which undergoes electrostatic binding with the amphiphile **4**. Consequently, care has to be taken if micelle formation is investigated with the help of only noncovalently bound fluorescence labels. Such guest molecules are not only spectators, but also play an active role in micelle formation. Cryo-TEM provides the direct visual evidence for a fundamental understanding of the spectroscopic data and reveals that the micellar structures formed by **4** are predominantly rod-shaped at pH 7 and solely spherical at pH 9. At the same time we found that exactly 12 molecules of **4** self-assemble to form a spherical and structurally persistent micelle at pH 7. The addition of pyrene did not influence the overall appearance of the aggregates at neutral pH. In contrast, at pH 9 the globular micelles are less uniform and most probably reflect the spatial demand of the guest molecules incorporated into the tightly packed micellar aggregates. Finally, at pH 4 an intriguing new kind of supramolecular architecture is observed. A membrane with a very uniform pattern of 5 nm pores expands the family of self-assembled structures, which is a subject of continuing research.

Experimental Section

All chemicals and solvents were purchased from Sigma-Aldrich and Acros Organics or were prepared according to literature procedures. Dendrimers were synthesized as described previously.[20] *tert*-Butylcalix[4]arene and 5,11,17,23-tetraamino-25,26,27,28-tetrakis(dodecyloxy)calix[4]arene were synthesized according to the methods of Gutsche and Iqbal.[21] All reactions were performed by using standard glassware. Dry solvents were prepared according to literature procedures. Reactions were monitored by thin-layer chromatography (TLC) using Riedel de Haën silica gel 60 F 254 aluminium foils and a UV lamp. The products were purified by flash chromatography (FC) on silica gel 60 (parcel size 0.04–0.063 nm) from Merck. ^{1}H and ^{13}C NMR spectra were recorded with Bruker Avance 300, JEOL JNM EX 400, JEOL JNM GX 400, and JEOL A 400 spectrometers. Solvent peaks were used as references. Resonance multiplicities are referred to as s (singlet), d (doublet), t (triplet), m (multiplet), and unresolved signals as br (broad). Mass Spectra were measured by using a Micromass Lab Spec (FAB) and a Finnigan MAT 900 spectrometer with 3-nitrobenzyl alcohol as the matrix. MALDI-TOF mass spectra were acquired on an AXIMA-CFR plus instrument (Kratos Analytical, Manchester, UK) with cinnamic acid as the matrix. UV/Vis spectrophotometry was performed on a Shimadzu UV-3102 spectrophotometer. Elemental analyses were performed by combustion and gas chromatography with an EA 1110 CHNS analyzer (CE Instruments). Fluorescence spectroscopy was performed on a Shimadzu RF-5301 PC Fluorescence spectrophotometer. Conductivity was measured with a Cond 340i handheld conductivity meter from WTW.

Sample preparation: All fluorescence samples for cmc determination were prepared in buffered solution made of ultrapure water from Fluka. The pH 7 Na/K buffer solution was prepared according to literature procedures.[22] The borate buffer solution was commercially available from Fluka. The concentration of pyrene and its derivatives was 6.0×10^{-7} mol L^{-1} in all sample solutions. To prepare the pyrene derivative stock solution a weighed amount was dissolved in acetone. A known amount of the pyrene/acetone solution was added to a 25 mL flask to adjust the concentration of pyrene to 6.0×10^{-7} mol L^{-1} and then the acetone was removed with gaseous nitrogen for 1 h. Then the flask was refilled with buffered water. To obtain a sample solution an amount of the pyrene/acetone stock solution was placed in a flask and the acetone blown off with nitrogen for 1 h. Then the sample dissolved in buffer was added and the mixture allowed to equilibrate for 1 h. With these freshly prepared solutions fluorescence measurements were performed with an excitation wavelength of 330 or 333 nm. The excitation and emission slit opening was 3 or 5 nm. The response time was 0.1 s and the scan time was 0.2 nm for all measurements. For the conductivity measurements, calixarene $\mathbf{4}^{12-}$ was completely deprotonated by dissolving the calixarene in water and adding 12 equivalents of sodium hydroxide.

Samples for electron microscopy were prepared from 2 mg mL^{-1} (7.5×10^{-4} mol L^{-1}) solutions of **4** in standard phosphate (pH 7) or borate buffer (pH 9). The samples of the loaded micelles were prepared as described for the fluorescence investigations with 2.65 mg mL^{-1} (10.0×10^{-4} mol L^{-1}, pH 7) and 2.76 mg mL^{-1} (10.4×10^{-4} mol L^{-1}, pH 9) solutions of **4**.

Electron cryomicroscopy: Droplets of the sample (5 μL) were applied to perforated (1 μm hole diameter) 200 mesh grids covered with a carbon film (R1/4 batch of Quantifoil, MicroTools GmbH, Jena, Germany), which had been hydrophilized before use by 60 s plasma treatment at 8 W in a Baltec Med 020 device. The supernatant fluid was removed with filter paper until an ultrathin layer of the sample solution was obtained spanning the holes of the carbon film. The samples were immediately vitrified by propelling the grids into liquid ethane at its freezing point (90 K) with a guillotine-like plunging device. The vitrified samples were subsequently transferred under liquid nitrogen into a Tecnai F20 transmission electron microscope (FEI, Oregon, USA) using the Gatan (Gatan Inc., California, USA) cryoholder and cryostage (Model 626). Microscopy was carried out at a sample temperature of 94 K by using the microscope's low dose routine. Images were recorded with a FEI Eagle 2k CCD camera at an accelerating voltage of 160 kV (binning: 1×; integration time: 1 s) at calibrated primary magnifications of 100000(×) and 62000×.

Cryonegative staining electron microscopy: Droplets of the sample (5 μL) were applied to 200 mesh copper grids covered with a carbon film, which had been hydrophilized before use by 60 s plasma treatment at 8 W in a Baltec Med 020 device. After 30 s the supernatant fluid was removed with filter paper. Subsequently, a droplet of staining solution (5 μL, phosphotungstic acid at pH 7) was applied for 45 s, blotted with filter paper, and the sample subsequently frozen in liquid ethane (see above). The vitrified samples were subsequently transferred under liquid nitrogen into a Philips CM12 transmission electron microscope (FEI, Oregon, USA) using the Gatan (Gatan Inc., California, USA) cryoholder and cryostage (Model 626). Microscopy was carried out at a sample temperature of 94 K using the low-dose protocol of the microscope at a primary magnification of 58300(×) and 300(×) and an accelerating voltage of 100 kV (LaB_6 illumination). All image processing and 3D reconstruction calculations of the image data were performed by using the Imagic 5 software (Image Science GmbH, Berlin, Germany), as described elsewhere.[1,3,4]

Synthesis of 5,11,17,23-tetraamino-25,26,27,28-tetrakis(dodecyloxy)calix[4]arene (5): 5,11,17,23-Tetranitro-25,26,27,28-tetrakis(dodecyloxy)calix[4]arene (3.76 g, 2.95 mmol) was dissolved in isopropanol (300 mL). Pd/C (379 g, 10%) and hydrazine hydrate (7.17 mL, 148 mmol) were added to this solution. The reaction mixture was stirred at reflux for 48 h. After cooling to 40 °C it was filtered through Celite and the residue washed with $CHCl_3$. The product was obtained after precipitation with

$CHCl_3$/MeOH in a yield of 86% as a light yellow powder (3.24 g, 2.54 mmol).

^{1}H NMR ($CDCl_3$, 400 MHz, RT): $\delta = 0.84$ (t, $^3J = 6.7$ Hz, 12H; CH_3), 1.23 (m, 72H; CH_2), 1.81 (m, 8H; CH_2), 2.87 (d, $^2J = 13.2$ Hz, 4H; CH_2), 3.71 (t, $^3J = 7.4$ Hz, 8H; CH_2), 4.26 (d, $^2J = 12.0$ Hz, 4H; CH_2), 6.02 ppm (s, 8H; CH_{arom}); ^{13}C NMR ($CDCl_3$, 100.5 MHz, RT): $\delta = 14.1$ (CH_3), 22.6, 25.0, 25.3, 26.4, 29.4, 29.7, 30.0, 30.2 (CH_2), 31.1 (CH_2-Ar), 31.9 (CH_2), 75.1 (CH_2-O), 115.7 (CH_{arom}), 135.6 (C_{arom}-CH_2), 140.2 (C_{arom}-NH), 150.0 ppm (C_{arom}-O); MS (FAB, NBA): m/z: 1158 $[M+H]^+$.

Synthesis of 5,11,17,23-tetrakis(4-methoxycarbonylphenylcarbonylamino)-25,26,27,28-tetrakis(dodecyloxy)calix[4]arene (7)

*Methyl 4-(chlorocarbonyl)benzoate (**6**):* Monomethyl terephthalate (929.0 mg, 5.16 mmol) was dissolved in thionyl chloride (16.3 mL, 137.0 mmol) and a drop of DMF was added. The mixture was stirred at 70°C for 4 h. The solvent was then removed and the product immediately used in the next reaction.

Amide formation: Methyl 4-(chlorocarbonyl)benzoate **6** (1.02 g, 5.1 mmol) was dissolved in THF (10 mL), triethylamine (1.43 μL, 10.32 mmol) added, and the mixture cooled to −10°C. 5,11,17,23-Tetraamino-25,26,27,28-tetrakis(dodecyloxy)calix[4]arene (**5**; 1.00 mg, 0.86 mmol) was dissolved in THF (10 mL) and added dropwise to the acid chloride mixture. After stirring for 8 h at ambient temperatures the solvent was removed under reduced pressure and the crude product was dissolved in $CHCl_3$ (25 mL) and washed with a saturated solution of $NaHCO_3$ (25 mL) and then brine (25 mL). The organic solution was dried over $MgSO_4$ and the pure product obtained after precipitation with $CHCl_3$ and MeOH as a yellow powder in a yield of 86% (1.33 g, 0.74 mmol).

^{1}H NMR ($CDCl_3$, 400 MHz, RT): $\delta = 0.86$ (t, $^3J = 6.0$ Hz, 12H; CH_3), 1.30 (m, 72H; CH_2), 1.89 (m, 8H; CH_2), 3.16 (d, $^2J = 13.4$ Hz, 4H; CH_2), 3.88 (m, 20H; OCH_2, OCH_3), 4.45 (d, $^2J = 13.4$ Hz, 4H; CH_2), 7.00 (s, 8H; CH_{arom}), 7.72 (d, $^3J = 8.5$ Hz, 8H; CH_{arom}), 7.87 (d, $^3J = 8.3$ Hz, 8H; CH_{arom}), 8.03 ppm (s, 4H; NH); ^{13}C NMR ($CDCl_3$, 100.5 MHz, RT): $\delta =$ 14.0 (CH_3), 22.6, 29.4, 29.7, 29.8, 29.82, 29.9, 30.0 (CH_2), 30.2, (CH_2-Ar), 31.1 (CH_2), 52.3 (O-CH_3), 75.4 (CH_2-O), 121.4 (CH_{arom}), 127.1 (CH_{arom}, benzyl), 129.7 (C_{arom}-NHCO), 131.6 (CH_{arom}, benzyl), 132.6 (C_{arom}-CO), 135.4 (C_{arom}-CH_2), 138.3 (C_{arom}-CONH), 154.1 (C_{arom}-O), 164.8, 166.2 ppm (CO); MS (FAB, NBA): m/z: 1806 $[M]^+$; elemental analysis calcd (%) for $C_{112.25}H_{148}D_{0.25}N_4O_{16}$·0.25 $CDCl_3$ (1836.49): C 73.41, H 8.15, N 3.05, O 13.94; found: C 73.19, H 8.19, N 3.18.

Synthesis of 5,11,17,23-tetrakis(carboxyphenylcarbonylamino)-25,26,27,28-tetrakis(dodecyloxy)calix[4]arene (8): Compound **7** (1.30 g, 0.74 mmol) was dissolved in THF (50 mL). H_2O (3 mL) and LiOH (142.0 mg, 5, 92 mmol) were added to this mixture. After 6 h at 60°C the reaction mixture was neutralized with 1 M HCl and then the solvent was removed and the product filtered and washed with water. After drying the product was obtained as a yellow powder in a yield of 95% (1.23 g, 0.70 mmol).

^{1}H NMR (DMSO, 400 MHz, RT): $\delta = 0.90$ (m, 12H; CH_3), 1.31–1,47 (m, 72H; CH_2), 2.04 (m, 8H; CH_2), 2.94 (brs, 4H; OH), 3.22 (d, $^2J = 12.8$ Hz, 4H; CH_2), 3.98 (t, $^3J = 7.5$ Hz, 8H; CH_2), 4.55 (d, $^2J = 12.8$ Hz, 4H; CH_2), 7.33 (s, 8H; CH_{arom}), 7.86–8.01 (m, CH, benzyl), 9.51 ppm (s, 4H; NH-CO); ^{13}C NMR (DMSO, 100.5 MHz, RT): $\delta = 14.6$ (CH_3), 23.7, 27.6, 30.6, 30.9, 31.0, 31.1, 31.2, 31.24, 31.3 (CH_2), 31.4 (CH_2-Ar), 33.1 (CH_2), 76.5 (CH_2-O), 121.4 (CH_{arom}), 128.5 (CH_{arom}, benzyl), 130.5 (C_{arom}-NHCO), 134.2 (CH_{arom}, benzyl), 134.7 (C_{arom}-CO), 135.8 (C_{arom}-CH_2), 140.5 (C_{arom}-CONH), 154.1 (C_{arom}-O), 165.1, 167.5 ppm (CO); elemental analysis calcd (%) for $C_{109}H_{140}DCl_3N_4O_{165}$·$CDCl_3$ (1870.67): C 69.98, H 7.65, N 3.00; found: C 69.73, H 7.71, N 3.31.

Synthesis of Newkome-type [G-1] 5,11,17,23-tetrakis(*tert*-butoxycarbonylphenylcarbonylamino)-25,26,27,28-tetrakis(dodecyloxy)calix[4]arene (9): Compound **8** (875.1 mg, 0.5 mmol) was dissolved in DMF (35 mL) and the solution cooled to 0°C. Then *N*′-(3-dimethylaminopropyl)-*N*-ethylcarbodiimide (EDC; 479.3 mg, 2.5 mmol), 4-dimethylaminopyridine (DMAP; 365.8 mg, 2.5 mmol), and 1-hydroxybenzotriazole (HOBt; 332.8 mg, 2.5 mmol) were added and the reaction mixture was stirred for 30 min. The first-generation Newkome dendrimer (1.66 g, 4 mmol) was added and the resulting solution stirred for 72 h. Then the solvent was removed and the crude dissolved in $CHCl_3$ (50 mL) and washed with citric acid (10%, 50 mL) and brine (50 mL). Reprecipitation with $CHCl_3$/MeOH furnished the product as a yellow powder in a yield of 58% (961.1 mg, 0.29 mmol).

^{1}H NMR ($CDCl_3$, 400 MHz, RT): $\delta = 0.87$ (m, 12H; CH_3), 1.25 (m, 72H; CH_2), 1.39 (s, 108H; CH_3, *t*Bu), 1.88 (m, 8H; CH_2), 2.13 (m, 24H; CH_2), 2.20 (m, 24H; CH_2), 3.17 (d, $^2J = 13.8$z, 4H; CH_2), 3.86 (t, $^3J = 7.5$ Hz, 8H; CH_2), 4.46 (d, $^2J = 13.6$ Hz, 4H; CH_2), 7.05 (s, 8H; CH_{arom}), 7.34 (s, 4H; NH), 7.82 (m, 8H; CH_{arom}, benzyl), 7.65 (m, 8H; CH_{arom}, benzyl), 8.14 (s, 4H; NH-CO); ^{13}C NMR ($CDCl_3$, 100.5 MHz, RT): $\delta = 14.0$ (CH_3), 22.6, 26.3 (CH_2), 28.0 (CH_3, *t*Bu), 29.4, 29.7, 29.76, 29.79, 29.9, 29.93, 30.1 (CH_2), 30.2, (CH_2-Ar), 31.9 (CH_2), 58.2 (C_q-NH), 75.4 (CH_2-O), 80.7 (CH_3, *t*Bu), 120.7 (CH_{arom}), 127.1 (CH_{arom}, benzyl), 127.4 (CH_{arom}, benzyl), 131.9 (C_{arom}-NHCO), 135.6 (C_{arom}-CO), 136.7 (C_{arom}-CH_2), 138.1 (C_{arom}-CONH), 154.1 (C_{arom}-O), 164.8, 165.9, 166.4 ppm (CO); MS (FAB, NBA): m/z: 3640 $[M+Na-2H]^+$; elemental analysis calcd (%) for $C_{196.17}H_{296}N_8O_{36}$·0.17 $CDCl_3$ (1833.41): C 70.10, H 8.89, N 3.33; found: C 69.78, H 8.81, N 3.51.

Synthesis of Newkome-type [G-2-OH] 5,11,17,23-tetrakis-[tris(carboxyethyl)methylaminocarbonylphenylcarbonylamino]-25,26,27,28-tetrakis(dodecyloxy)calix[4]arene (4): Compound **9** (831.0 mg, 0.25 mmol) was dissolved in formic acid (63 mL) and stirred for 12 h. Then the solvent was removed and the product dried under reduced pressure to furnish the product as a beige powder in a yield of 91% (605.0 mg, 0.23 mmol).

^{1}H NMR ($CDCl_3$, 400 MHz, RT): $\delta = 0.87$ (m, 12H; CH_3), 1.28–1.42 (m, 80H; CH_2), 2.02 (m, 24H; CH_2), 2.20 (m, 24H; CH_2), 3.23 (d, $^2J =$ 12.5 Hz, 4H; CH_2), 3.94 (t, $^3J = 7.3$ Hz, 8H; CH_2), 4.48 (d, $^2J = 12.0$ Hz, 4H; CH_2), 7.34 (s, 8H; CH_{arom}), 7.57 (s, 4H; NH), 7.82 (d, $^3J = 8.0$ Hz, 8H; CH_{arom}, benzyl), 7.92 (d, $^3J = 8.0$ Hz, 8H; CH_{arom}; benzyl); ^{13}C NMR ($CDCl_3$, 100.5 MHz, RT): $\delta = 13.8$ (CH_3), 22.2, 26.1, 28.2, 29.0, 29.4, 29.5, 29.6, 29.7, 29.8, 30.0, 31.5 (CH_2), 57.5 (C_q-NH), 75.2 (CH_2-O), 121.3 (CH_{arom}), 127.4 (CH_{arom}, benzyl), 133.3 (C_{arom}-NHCO), 134.2 (C_{arom}-CO), 137.6 (C_{arom}-CH_2), 137.9 (C_{arom}-CONH), 152.5 (C_{arom}-O), 164.5, 166.1, 174.7 ppm (CO); MS (MALDI-TOF, cinnamic acid): m/z: 2689.4 $[M+Na-H]^+$; elemental analysis calcd (%) for $C_{148.3}H_{200}D_{0.3}Cl_{0.9}N_8O_{36}$·0.3 $CDCl_3$ (2703.32): C 65.89, H 7.48, N 4.15; found: C 65.70, H 7.52, N 4.37.

Synthesis of 1-(4-bromobutyl)pyrene (12): PPh_3 (816.00 mg, 3.11 mmol) was added to a solution of 4-pyren-1-ylbutanol (**11**; 712.00 mg, 2.60 mmol) and CBr_4 (2.65 mg, 5.30 mmol) in CH_2Cl_2 (20 mL). After 6 min the reaction was quenched with Na_2CO_3 (55 mL). After extracting the aqueous phase three times with CH_2Cl_2 (20 mL), the combined organic phases were washed with Na_2CO_3 (20 mL) twice. Column chromatography with cyclohexane/EtOAc (96:4) furnished the light-sensitive product in a yield of 70% (625.12, 1.80 mmol).

^{1}H NMR (300 MHz, $CDCl_3$, RT): $\delta = 2.01$ (m, 4H; CH_2), 3.35 (m, 2H; CH_2), 3.45 (m, 4H; CH_2), 7.84 (d, $^3J = 7.9$ Hz, 1H; CH), 7.99 (m, 3H; CH_{arom}), 8.14 (m, 4H; CH_{arom}), 8.25 ppm (d, $^3J = 9.2$ Hz, 1H; CH); ^{13}C NMR (300 MHz, $CDCl_3$, RT): $\delta = 30.2$, 32.55, 32.6, 33.6 (CH_2), 123.2, 124.7, 124.8, 124.9, 125.0, 125.04, 125.8, 126.6, 127.2 (CH_{arom}), 127.3, 127.5, 128.6, 129.9, 130.8, 131.4, 136.0 ppm (C_q-Ar); MS (FAB, NBA): m/z: 338 $[M+H]^+$; elemental analysis calcd (%) for $C_{20}H_{17}Br$ (337.25): C 71.23, H 5.08; found: C 71.32, H 5.12.

Synthesis of 1-(4-trimethylammoniobutyl)pyrene bromide (10): 1-(4-Bromobutyl)pyrene (**12**; 300.00 mg, 0.86 mmol) was dissolved in THF (5 mL) and NMe_3 (2 mL, 50%) was added, whereupon a yellow precipitate formed. The mixture was stirred for 8 h and then the solvent was removed. The crude product was reprecipitated with EtOH/Et_2O. Filtration and drying under reduced pressure furnished the product as a yellow powder in a yield of 10%.

^{1}H NMR (300 MHz, $CDCl_3$, RT): $\delta = 1.69$ (m, 2H; CH_2), 1.83 (m, 2H; CH_2), 3.22 (s, 6H; CH_3), 3.33 (t, $^3J = 7.3$ Hz, 2H; CH_2), 3.52 (m, 2H; CH_2) 7.80 (d, $^3J = 7.8$ Hz, 1H; CH), 7.95 (m, 3H; CH_{arom}), 8.09 (m, 4H; CH_{arom}), 8.17 ppm (d, $^3J = 9.2$ Hz, 1H; CH); ^{13}C NMR (300 MHz, $CDCl_3$, RT): $\delta = 22.6$, 27.7, 32.4 (CH_2), 53.2 (CH_3), 66.4 (CH_2-NH), 123.2, 124.9, 125.0, 125.05, 125.1, 126.1, 126.9, 127.4 (CH-Py), 127.5, 127.7, 128.6,

130.1, 130.8, 131.4, 135.0 ppm (C_q-Ar); MS (FAB, NBA): *m*/*z*: 316 $[M-Br]^+$; elemental analysis calcd (%) for $C_{23}H_{26}N$ (396.36): C 67.70, H 6.61, N 3.53; found: C 69.78, H 6.55, N 3.51.

Acknowledgements

We thank the Deutsche Forschungsgemeinschaft (B0 1000/6-1 to C.B and HI 468/13-2 as well as Cluster of Excellence: Engineering of Advanced Materials to A.H.) for financial support.

[1] a) M. Kellermann, W. Bauer, A. Hirsch, B. Schade, K. Ludwig, C. Boettcher, *Angew. Chem.* **2004**, *116*, 3019; *Angew. Chem. Int. Ed.* **2004**, *43*, 2959; b) M. Kellermann, W. Bauer, A. Hirsch, B. Schade, K. Ludwig, C. Böttcher, *Angew. Chem.* **2004**,*116*, 3019; *Angew. Chem. Int. Ed.* **2004**, *43*, 2959.
[2] Y. Chang, M. Kellermann, M. Becherer, A. Hirsch, C. Bohne, *Photochem. Photobiol. Sci.* **2007**, *6*, 525.
[3] a) S. Burghardt, A. Hirsch, B. Schade, K. Ludwig, C. Böttcher. *Angew. Chem.* **2005**, *117, 3036; Angew. Chem. Int. Ed.* **2005**, 44, 2976; *Angew. Chem. Int. Ed.* **2005**, *44*, 2976.
[4] U. Hartnagel, D. Balbinot, N. Jux, A. Hirsch. *Org. Biomol. Chem.* **2006**, *36*, 1785; a) B. Schade, K. Ludwig, C. Böttcher, U. Hartnagel, A. Hirsch. *Angew. Chem.* **2007**, *119*, 4482; b) B. Schade, K. Ludwig, C. Böttcher, U. Hartnagel, A. Hirsch, *Angew. Chem.* **2007**, *119*, 4472; *Angew. Chem. Int. Ed.* **2007**, 46, 4393.
[5] S. Lucht, J. Stumpe, M. Rutloh, *J. Fluorescence* **1998**, *8*, 153.
[6] J. Heldt, D. Gormin, M. Kasha, *Chem. Phys. Lett.* **1988**, *150*, 433.
[7] F. Sansone, M. Dudic, G. Donofrio, C. Rivetti, L. Baldini, A. Casnati, S. Cellai, R. Ungaro, *J. Am. Chem. Soc.* **2006**, *128*, 14528.
[8] K. Furuta, K. Tomokiyo, M. T. Kuo, T. Ishikawa, M. Suzuki, *Tetrahedron* **1999**, *55*, 7529.
[9] G. P. L′Heureux, M. Fragata, *Biophys. Chem.* **1988**, *30*, 293.
[10] The benzamide intensity (I_{BA}) was normalized to the highest measured intensity ($I_{BA,max}$) at the corresponding pH value.
[11] E. Fuguet, C. Rafols, M. Roses, E. Bosch, *Anal. Chim. Acta* **2005**, *548*, 95.
[12] The straight lines were linear fitted to the linear slopes at low (8×10^{-6} to 8×10^{-13} mol L^{-1}) and high (1×10^{-4} to 9×10^{-4} mol L^{-1}) concentrations of **4** using the program ORIGIN. This method was established to quantify the fluorescence quenching induced by the interaction between **4** and the pyrene derivatives.
[13] a) A. Bernheim-Groswasser, R. Zana, Y. Talmon, *J. Phys. Chem. B* **2000**, *104*, 4005; b) P. R. Majhi, P. L. Dubin, X. Feng, X. Guo, *J. Phys. Chem. B* **2004**, *108*, 5980.
[14] The final resolution achieved in the reconstruction of 11041 individual aggregates of **4** was determined by the Fourier shell correlation method (FSC) (see ref. [14a]) and amounts to about 9.8 Å on the basis of the 3σ threshold criterion (≈13.7 Å at 0.5 criterion) and the D_2 point-group symmetry (see ref. [14b]); a) G. Harauz, M. van Heel, *Optic* **1986**, *73*, 146; b) E. V. Orlova, P. Dube, J. R. Harris, E. Beckmann, F. Zemlin, J. Markl, M. v. Heel, *J. Mol. Biol.* **1997**, *271*, 417.
[15] J.-K Kim, E. Lee, Y. B. Lim, M. Lee, *Angew. Chem.* **2008**, *120*, 4818; *Angew. Chem. Int. Ed.* **2008**, *47*, 4740.
[16] a) K. Kalyanasundaram, J. K. Thomas, *J. Am. Chem. Soc.* **1977**, *99*, 2039; b) K. Kalyanasundaram, J. K. Thomas, *J. Phys. Chem. Soc.* **1977**, *81*, 2176.
[17] G. M. L. Consoli, G. Granata, R. Lo Nigro, G. Malandrino, C. Geraci, *Langmuir* **2008**, *24*, 6194.
[18] G. Pistolis, A. Malliaris, D. Tsiourvas, C. M. Paleos, *Chem. Eur. J.* **1999**, *5*, 1440.
[19] The cmcs of **10** and **13** were determined by diluting them in buffer at the corresponding pH. Plotting the development of the intensity I_1 of the pyrene moiety versus the concentrations of **10** and **13** revealed a nonlinear concentration dependence with the concentration at the maximum intensity representing the cmc.
[20] M. Brettreich, A. Hirsch, *Synlett* **1998**, 1396.
[21] D. Gutsche, M. Iqbal, *Org. Synth.* **1989**, *68*, 234.
[22] F. W. Küster, A. Thiel, *Rechentafeln für die Chemische Analytik*, 102nd ed., de Gryter, Berlin, New York, **2002**.

Received: September 29, 2008
Published online: January 2, 2009

